

# Empirical study of formamide formation around young O-type stars

V. Allen<sup>1,2,3</sup>, A. López-Sepulcre<sup>4,5</sup>, Á. Sánchez-Monge<sup>6</sup>,  
V. M. Rivilla<sup>7</sup>, and R. Cesaroni<sup>7</sup>

<sup>1</sup> NASA Goddard Space Flight Center, 8800 Greenbelt Road, Greenbelt, MD 20771, USA  
e-mail: [veronica.a.allen@nasa.gov](mailto:veronica.a.allen@nasa.gov)

<sup>2</sup> Kapteyn Astronomical Institute, Landleven 12, 9747 AD Groningen, the Netherlands

<sup>3</sup> SRON, Landleven 12, 9747 AD Groningen, the Netherlands

<sup>4</sup> CNRS, IPAG, Univ. Grenoble Alpes, 414 Rue de la Piscine, 38000 Saint-Martin-d'Hères, France

<sup>5</sup> IRAM, 300 rue de la Piscine, 38406 Saint-Martin d'Hères, France

<sup>6</sup> I. Physikalisches Institut, Universität zu Köln, Zùlpicher Strasse 77, 50937 Köln, Germany

<sup>7</sup> INAF-Osservatorio Astrofisico di Arcetri, Largo Enrico Fermi 5, I-50125 Florence, Italy

**Abstract.** Formamide ( $\text{NH}_2\text{CHO}$ ) is an important prebiotic molecule as it has been proposed as a precursor to amino acids and other important molecules of life. In my talk, I detail the results of a high angular resolution ( $0.2''$ ) ALMA observations of several different young high-mass stars and how the spatial extent and kinematics of formamide ( $\text{NH}_2\text{CHO}$ ) in the surrounding gas compares to two of its possible parent species isocyanic acid ( $\text{HNCO}$ ) and formaldehyde ( $\text{H}_2\text{CO}$ ). This is important astrochemical work because there is debate about whether formamide is formed in ice and melts off once it becomes warm (from  $\text{HNCO}$ ) or in already warm gas (from  $\text{H}_2\text{CO}$ ). The results of this pilot study will be followed up with future ALMA observations.

**Key words.** stars: massive – ISM: individual objects: G17.64+0.16, G24.78+0.08, G345.49+1.47 – astrochemistry

## 1. Introduction

Formamide ( $\text{NH}_2\text{CHO}$ ) is an important molecular species to study as it is thought to be a precursor to the simplest amino acid, glycine ( $\text{NH}_2\text{CH}_2\text{COOH}$ ) (Saladino et al. 2012). The peptide bond ( $\text{N-C=O}$ ) makes  $\text{NH}_2\text{CHO}$  especially relevant to astrobiology as pre-biotic molecules were likely delivered to an early Earth to help bring about the origin of life. As for formamide itself, there is disagreement about how it forms. Here we investigate two

formation routes: (1) hydrogenation of isocyanic acid ( $\text{HNCO}$ ) on dust grain ice mantles in the reactions  $\text{HNCO} + \text{H} \rightarrow \text{H}_2\text{NCO}$  then  $\text{H}_2\text{NCO} + \text{H} \rightarrow \text{NH}_2\text{CHO}$  (Charnley, S. B. 1997) which later sublimates into the gas or (2) reactions between  $\text{H}_2\text{CO}$  and  $\text{NH}_2$  (which is especially abundant in photon-dominated regions) in warm gas ( $\text{H}_2\text{CO} + \text{NH}_2 \rightarrow \text{NH}_2\text{CHO} + \text{H}$ ) (Kahane et al. 2013) (see Figure 1 for a visual illustration).

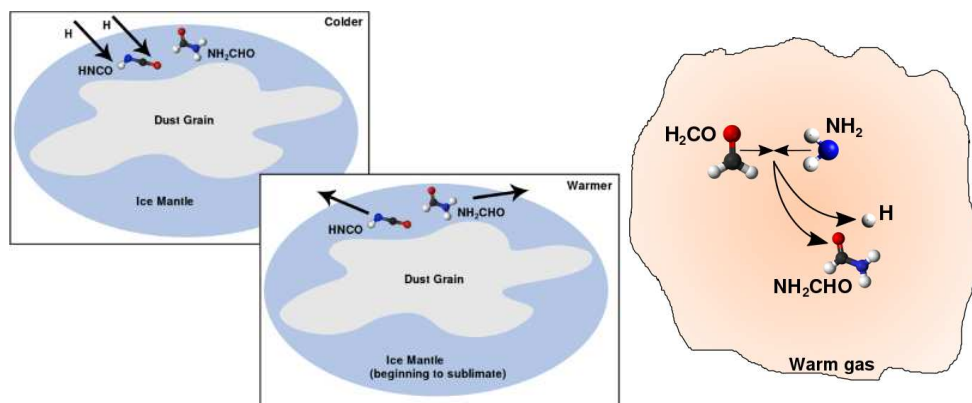


**Fig. 1.** Illustrations of the formation reactions for  $\text{NH}_2\text{CHO}$ . Hydrogenation of  $\text{HNCO}$  (left) and  $\text{H}_2\text{CO} + \text{NH}_2$  (right).

Evidence has been presented supporting both formation pathways. Recent laboratory work by Kaňuchová et al. (2017) shows that  $\text{NH}_2\text{CHO}$  can be formed in cosmic-ray-irradiated ices but the  $\text{HNCO}/\text{NH}_2\text{CHO}$  ratio does not match observations. A tight empirical correlation between the abundances of  $\text{HNCO}$  and  $\text{NH}_2\text{CHO}$  has been observed using single dish observations (López-Sepulcre et al. 2015; Mendoza et al. 2004). This correlation between the abundances of these species is nearly linear and spans several orders of magnitude, suggesting that the two molecules are chemically related. ALMA observations by Coutens et al. (2016) of IRAS 16293-2422 show that the deuterium fractions in  $\text{HNCO}$  and  $\text{NH}_2\text{CHO}$  are very similar, also implying a chemical link.

On the other hand, the laboratory study by Noble et al. (2015) finds that hydrogenation of  $\text{HNCO}$  by deuterium bombardment does not lead to  $\text{NH}_2\text{CHO}$  in detectable quantities, while Barone et al. (2015) find that the  $\text{H}_2\text{CO} + \text{NH}_2$  reaction can reproduce the abundance of  $\text{NH}_2\text{CHO}$  in IRAS16293-2422, a Sun-like protostar. Codella et al. (2017) observed a shock near L1157-B1 using interferometric observations. Through these observations and follow-up chemical modeling, they concluded that  $\text{NH}_2\text{CHO}$  is made efficiently in the gas phase from  $\text{H}_2\text{CO}$ , at least in this source. Recent work by Quénard et al. (2018) modeling the formation of  $\text{HNCO}$  and

$\text{NH}_2\text{CHO}$  and other peptide-bearing molecules shows a correlation between the abundances of  $\text{H}_2\text{CO}$  and  $\text{NH}_2\text{CHO}$  as well as between  $\text{HNCO}$  and  $\text{NH}_2\text{CHO}$  without using hydrogenation. The possibility exists that different types of sources (shocked regions, outflow cavities, accretion disks, protostellar envelopes, etc.) may have different dominant formation routes, but this possibility stands to be examined.

## 2. Observational tests

### 2.1. Moment maps

Using ALMA Cycle 2 observations of three high-mass star-forming regions (shown in Figure 2) with six sub-sources (listed in Table 1) containing young O-type stars, we studied moment maps (integrated intensity, velocity, and velocity dispersion) of 1-3 transitions each of  $\text{HNCO}$ ,  $\text{H}_2\text{CO}$ , and  $\text{NH}_2\text{CHO}$  (all transitions studied are listed in Table 2) comparing the emission peak position, velocity gradient, and gas velocity dispersion. Comparisons were made under the assumption that similarities in gas peak, velocity gradient, and dispersion imply that the compared species are in the same gas and are therefore chemically related.

In these conference proceedings, we present the analysis of G345 as an example. The full report can be found in Allen et al.

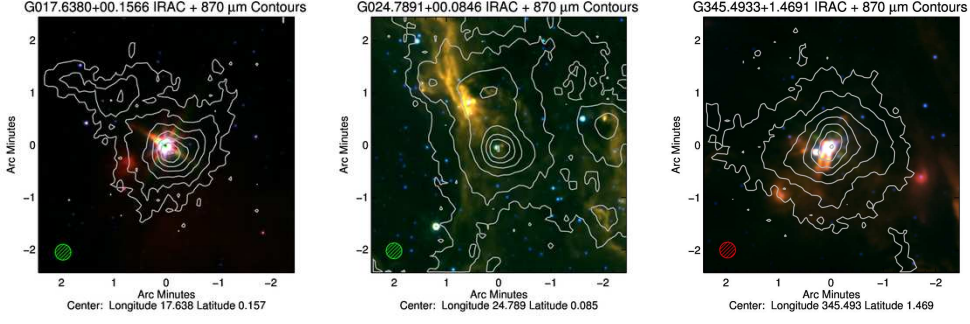


**Fig. 2.** Spitzer IRAC images overlaid with ATLASGAL contours of the star forming regions: (left) G17.64+0.16, (center) G24.78+0.08, and (right) G345.49+1.47 (from RMS database).

**Table 1.** Spectral extraction points for line identification and spectral modeling. These points coincide with the  $\text{NH}_2\text{CHO}$  peak used for each source.  $N_{\text{core}}$  is determined as in Sánchez-Monge et al. (2014) using the continuum intensity at the spectral extraction point assuming a  $T_{\text{ex}}$  of 100 K, a dust opacity of  $1.75 \text{ cm}^2 \text{ g}^{-1}$ , and a gas-to-dust ratio of 100. Check mark ( $\checkmark$ ) symbols indicate the detection of  $\text{H}(30)\alpha$  emission toward the sub-source.

Source	Right Ascension (J2000)	Declination (J2000)	$N_{\text{core}}$ ( $\text{cm}^{-2}$ )	$\text{H}(30)\alpha$
G17	18:22:26.370	-13:30:12.06	$2.8 \times 10^{25}$	$\checkmark$
G24 A1	18:36:12.544	-07:12:11.14	$9.1 \times 10^{24}$	$\checkmark$
G24 A2(N)	18:36:12.465	-07:12:09.61	$1.7 \times 10^{24}$	
G24 A2(S)	18:36:12.471	-07:12:10.09	$1.4 \times 10^{24}$	
G345 main	16:59:41.628	-40:03:43.63	$2.3 \times 10^{26}$	$\checkmark$
G345 NW spur	16:59:41.586	-40:03:43.15	$4.5 \times 10^{25}$	

**Table 2.** Transition properties from the CDMS (Endres et al. 2016). The last column shows the sources in which this transition appeared.  $\text{HNCO}$  (3) has a much higher upper energy level than the other transitions, so we consider it cautiously.

Species	Transition	Frequency (MHz)	$E_{\text{up}}$ (K)	$A_{ij}$ ( $\text{s}^{-1}$ )	Sources
$\text{HNCO}$ (1)	$10_{0,10}-9_{0,9}$	219798.27	58.0	$1.47 \times 10^{-4}$	G24
$\text{HNCO}$ (2)	$10_{1,9}-9_{1,8}$	220584.75	101.5	$1.45 \times 10^{-4}$	G17, G345
$\text{HNCO}$ (3)	$10_{3,7}-9_{3,6}$	219656.77	432.9	$1.20 \times 10^{-4}$	G24, G345
$\text{NH}_2\text{CHO}$ (1)	$10_{1,9}-9_{1,8}$	218459.21	60.8	$7.47 \times 10^{-4}$	G17, G345
$\text{NH}_2\text{CHO}$ (2)	$11_{2,10}-10_{2,9}$	232273.64	78.9	$8.81 \times 10^{-4}$	G24
$\text{H}_2\text{CO}$ (1)	$3_{0,3}-2_{0,2}$	218222.19	20.9	$2.82 \times 10^{-4}$	G17, G24, G345
$\text{H}_2\text{CO}$ (2)	$3_{2,2}-2_{2,1}$	218475.63	68.1	$1.57 \times 10^{-4}$	G17, G24, G345
$\text{H}_2\text{CO}$ (3)	$3_{2,1}-2_{2,0}$	218760.07	68.1	$1.58 \times 10^{-4}$	G17, G24, G345

2019 (in review). G345 can be divided into two sub-sources: Main, which shows very strong continuum, weak  $\text{H}(\alpha)$  emission, and little chemical complexity; and NW spur,

which is very chemically complex but has very weak continuum emission. Figure 3 shows the contours  $\text{H}_2\text{CO}$  and  $\text{HNCO}$  vs.  $\text{NH}_2\text{CHO}$ . The difference between the emis-

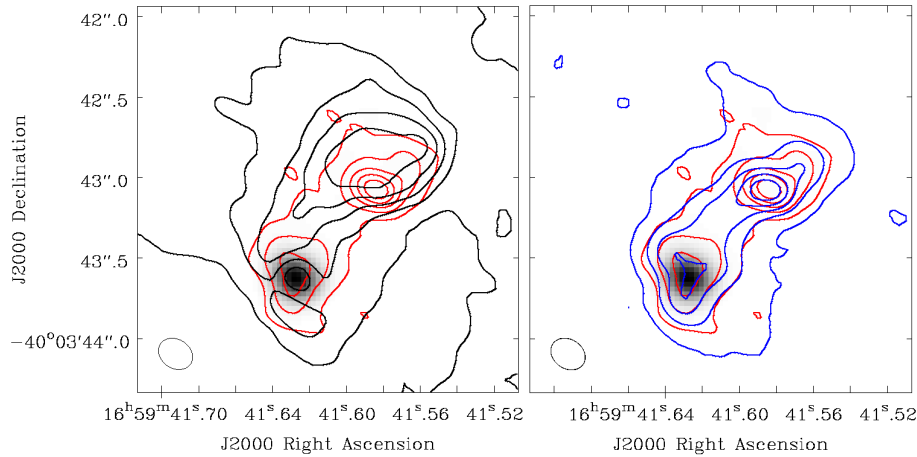


**Fig. 3.** G345 moment 0 maps (contours) overlaid on the dust continuum (greyscale). *Left:* the black contours show the  $\text{H}_2\text{CO}$  (3) transition ( $E_{\text{up}}=68.1$  K) from  $5\sigma$  ( $0.027$  Jy/beam  $\text{km s}^{-1}$ ) to a peak of  $0.402$  Jy/beam  $\text{km s}^{-1}$ . The red contours show  $\text{NH}_2\text{CHO}$  (1) emission ( $E_{\text{up}}=60.8$  K) from  $5\sigma$  ( $0.020$  Jy/beam  $\text{km s}^{-1}$ ) to  $0.242$  Jy/beam  $\text{km s}^{-1}$ . *Right:* the blue contours show the extent of the  $\text{HNC}$  (2) emission ( $E_{\text{up}}=101.5$  K) from  $5\sigma$  ( $0.014$  Jy/beam  $\text{km s}^{-1}$ ) to  $0.428$  Jy/beam  $\text{km s}^{-1}$  with the red contours showing  $\text{NH}_2\text{CHO}$  (as in the left frame).

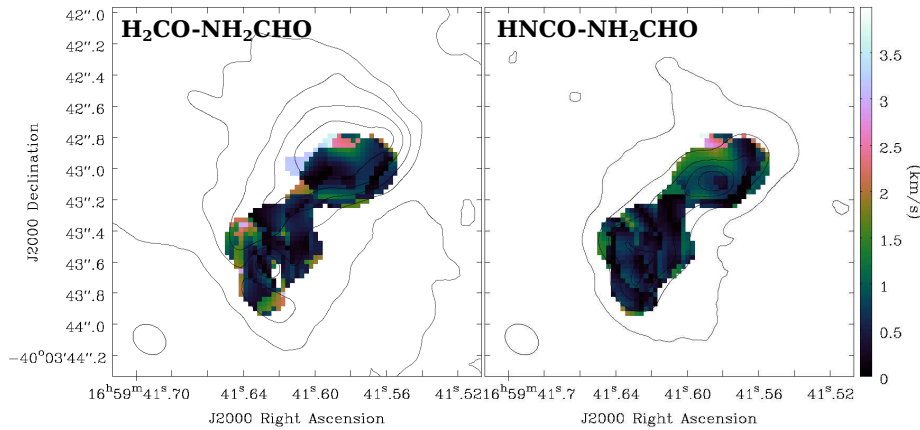


**Fig. 4.** Velocity difference (from moment 1 maps) at each pixel in G345 between (left)  $\text{H}_2\text{CO}$  (2) and  $\text{NH}_2\text{CHO}$  (1) and (right)  $\text{HNC}$  (2) and  $\text{NH}_2\text{CHO}$  (1). The contours show the integrated intensity maps for  $\text{H}_2\text{CO}$  (2) and  $\text{HNC}$  (2) as in Figure 3. The velocity scale is the same for both panels.

sion peaks for G345 Main were  $\sim 0.2''$  for  $\text{H}_2\text{CO}$  and  $\text{NH}_2\text{CHO}$  and  $\sim 0.04$  for the  $\text{HNC}$  (2) and  $\text{NH}_2\text{CHO}$ . For G345 NW spur, these differences were  $0.2''$  and  $0.03''$ , respectively. Figure 4 shows the difference in velocity values ( $v_{\text{H}_2\text{CO}} - v_{\text{NH}_2\text{CHO}}$  (left) and  $v_{\text{HNC(2)}} - v_{\text{NH}_2\text{CHO}}$  (right)) for each pixel with darker colors indicating a small difference and

lighter colors a greater difference. For G345, the moment maps of  $\text{HNC}$  are more similar to  $\text{NH}_2\text{CHO}$  than those of  $\text{H}_2\text{CO}$ . We see from the summary of map analysis results in Table 3 that the peak positions and dispersion maps favor  $\text{HNC}$  slightly over  $\text{H}_2\text{CO}$  in similarity with  $\text{NH}_2\text{CHO}$  and the velocity dispersion maps for  $\text{HNC}$  are almost always

most similar to  $\text{NH}_2\text{CHO}$ . From these overall results, it seems that  $\text{HNCO}$  has a slightly stronger relationship with  $\text{NH}_2\text{CHO}$ .

## 2.2. Spectral line modeling

In addition to analyzing the moment maps, we also used the XCLASS<sup>1</sup> spectral line modeling software (Möller et al. 2017) assuming local thermal equilibrium (LTE) to determine the excitation temperature ( $T_{\text{ex}}$ ), column density ( $N_{\text{col}}$ ), line width (FWHM), and velocity offset ( $v_{\text{LSR}}$ ) for each of our focus species and compare them to each other. This software models the data by solving the radiative transfer equation for an isothermal object in one dimension, taking into account source size and dust opacity.

Comparing the model results obtained using spectra extracted from pixels coinciding with the  $\text{NH}_2\text{CHO}$  emission peaks, we found no significant relationship between  $T_{\text{ex}}$  values, or FWHM of the three species. There was a strong relationship ( $R^2=0.93$  where 1 is perfectly correlated) between the abundances ( $X$ ; the modeled  $N_{\text{col}}$  value divided by the  $N_{\text{core}}$  value calculated from the dust continuum) of  $\text{HNCO}$  and  $\text{NH}_2\text{CHO}$ . This relationship was previously investigated by López-Sepulcre et al. (2015) whose best power-law fit equation from that paper was reported to be  $X(\text{NH}_2\text{CHO}) = 0.04 X(\text{HNCO})^{0.93}$ . Figure 5 shows that the best fit in this work is  $X(\text{NH}_2\text{CHO})=0.03(\pm 0.02) X(\text{HNCO})^{0.92(\pm 0.08)}$  and that correlations can be found between each pair of species abundances, but the strongest, by far, is that of  $\text{HNCO}$  and  $\text{NH}_2\text{CHO}$ . There is also a stronger correlation between the velocity shifts of  $\text{HNCO}$  and  $\text{NH}_2\text{CHO}$  than  $\text{H}_2\text{CO}$  and  $\text{NH}_2\text{CHO}$  ( $R^2$  of 0.95 vs. 0.48).

## 2.3. Caveats and future work

The opacity of the  $\text{H}_2\text{CO}$  transitions investigated here cannot be discounted. It is possible that the greater differences in spatial distribu-

tion, velocity, and dispersion between  $\text{H}_2\text{CO}$  and  $\text{NH}_2\text{CHO}$  compared to  $\text{HNCO}$  arise from optical depth issues. This is being investigated in a follow-up study involving isotopologues. It can also be seen in Table 3 that many of the moment map differences between each potential parent species and  $\text{NH}_2\text{CHO}$  are the equal within errors. This will be remedied in the future by using higher spatial and velocity resolution observations.

## 3. Conclusions

We present an observational study of two species that are potentially chemically related ( $\text{HNCO}$  and  $\text{H}_2\text{CO}$ ) to  $\text{NH}_2\text{CHO}$ . In our spectral modeling, we confirm the single dish relationship between the abundances of  $\text{HNCO}$  and  $\text{NH}_2\text{CHO}$  demonstrated in López-Sepulcre et al. (2015) using interferometric observations. Our map analyses favor  $\text{HNCO}$  as chemically related to  $\text{NH}_2\text{CHO}$ . The abundance correlation between  $\text{HNCO}$  and  $\text{NH}_2\text{CHO}$  is stronger than the correlation between  $\text{H}_2\text{CO}$  and  $\text{NH}_2\text{CHO}$  but both are well correlated. It is possible that both formation processes are important in creating this species, or that different environments favor one process over the other. Dedicated studies using more transitions and isotopologues in a more diverse selection of sources (high- and low-mass protostars, young stellar objects with disks, outflow regions, etc.) will shed light on this relationship.

*Acknowledgements.* This work makes use of ALMA data: ADS/JAO.ALMA 2013.1.00489.S (P.I. Riccardo Cesaroni). ALMA is a partnership of ESO (representing its member states), NSF (USA) and NINS (Japan), together with NRC (Canada) and NSC and ASIAA (Taiwan), in cooperation with the Republic of Chile. The Joint ALMA Observatory is operated by ESO, AUI/NRAO and NAOJ. The PhD project of V. Allen was funded by NWO and SRON. V. Allen's research is supported by an appointment to the NASA Postdoctoral Program at the NASA Goddard Space Flight Center, administered by Universities Space Research Association under contract with NASA. V.M.R. is funded by the the European Union's Horizon 2020 research and innovation programme under the Marie Skłodowska-Curie grant agreement No 664931.

<sup>1</sup> Available from: <https://xclass.astro.uni-koeln.de/>

**Table 3.** Summary of results from map analyses. The check symbol (✓) indicates the species with the emission peak closest to the NH<sub>2</sub>CHO peak, velocity-difference histogram center nearest to zero, or dispersion-difference histogram center nearest to zero. Equals signs (=) indicate that the parameters were equal for both HNC and H<sub>2</sub>CO within errors.

Source	HNC			H <sub>2</sub> CO		
	Peak	Velocity	Dispersion	Peak	Velocity	Dispersion
G17		=	✓	✓	=	
G24 A1	✓	✓	✓			
G24 A2(N)	✓		✓		✓	
G24 A2(S)	=	=	✓	=	=	
G345 Main	✓	=	✓		=	
G345 NW spur	✓	=	=		=	=

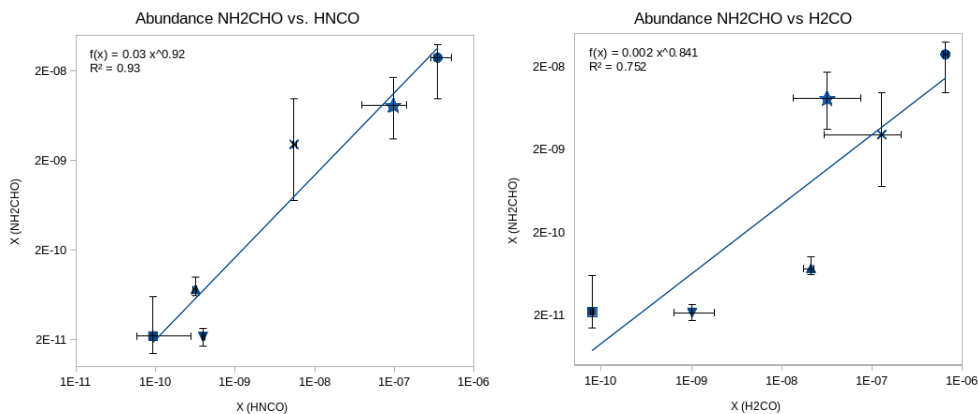


**Fig. 5.** XCLASS determined abundance comparison between NH<sub>2</sub>CHO and HNCO (left), NH<sub>2</sub>CHO and H<sub>2</sub>CO (right). The symbols correspond to different regions as follows: G17 is an upward triangle, G24 A1 is an 'x', G24 A2(N) is a star, G24 A2(S) is a circle, G345 main is a square, and G345 NW spur is a downward triangle.

## References

- Barone, V., Latouche, C., Skouteris, D., et al. 2015, MNRAS, 453, L31
- Charnley, S. B. 1997, in *Astronomical and Biochemical Origins and the Search for Life in the Universe*, eds. C. Batalli Cosmovici, et al. (Editrice Compositori, Bologna), IAU Colloquium, 161, 89
- Codella, C., Ceccarelli, C., Caselli, P., et al. 2017, A&A, 605, L3
- Coutens, A., Jørgensen, J. K., van der Wiel, M. H. D., et al. 2016, A&A, 590, L6
- Endres, C. P., Schlemmer, S., Schilke, P., et al. 2016, J. Mol. Spectrosc., 327, 95
- Kahane, C., Ceccarelli, C., Faure, A., & Caux, E. 2013, ApJ, 763, L38
- Kaňuchová, Z., Boduch, P., Domaracka, A., et al. 2017, A&A, 604, 68
- López-Sepulcre, A., Jaber, A. A., Mendoza, E., et al. 2015, MNRAS, 449, 2438
- Mendoza, E., Lefloch, B., López-Sepulcre, A., et al. 2014, MNRAS, 445, 151
- Möller, T., Endres, C. & Schilke, P. 2017, A&A, 598, A7
- Noble, J. A., Theule, P., Congiu, E., et al. 2015, A&A, 576, A91
- Quénard, D., Jiménez-Serra, I., Viti, S., et al. 2018, MNRAS, 474, 2796
- Saladino, R., Crestini, C., Pino, S., et al. 2012, Physics of Life Reviews, 9, 84
- Sánchez-Monge, Á., Beltrán, M. T., Cesaroni, R., et al. 2014, A&A, 569, A11